

Thermodynamics of a one-dimensional $S = 1/2$ spin-orbital model

J. Sirker*

School of Physics, The University of New South Wales, Sydney 2052, Australia

(Dated: November 11, 2018)

The thermodynamic properties of a one-dimensional model describing spin dynamics in the presence of a twofold orbital degeneracy are studied numerically using the transfer-matrix renormalization group (TMRG). The model contains an integrable $SU(4)$ -symmetric point and a gapless phase which is $SU(4)$ invariant up to a rescaling of the velocities for spin and orbital degrees of freedom which allows detailed comparison of the numerical results with conformal field theory. We pay special attention to the correlation lengths which show an intriguing evolution with temperature. We find that the model shows an intrinsic tendency towards dimerization at finite temperature even if the ground state is not dimerized.

PACS numbers: 75.10Jm, 05.70.-a, 05.10.Cc

I. INTRODUCTION

Contrary to a usual band insulator the internal degrees of freedom remain still active in a *Mott insulator*. In most of these insulators the spatial distribution of electrons around every atom is frozen in at the melting point and changes little down to zero temperature so that the spin is the only active internal degree of freedom. This leads to the widely studied spin models as for example the Heisenberg model or the t-J model when hole-doping away from the insulating case is studied. In recent years, however, there has been considerable interest in systems which have additional *orbital degrees of freedom* so that the spatial distribution of electrons (orbital order) may change considerably with temperature.^{1,2} Transition-metal oxides where orbitals are believed to play an important role are for example LaMnO_3 ^{2,3,4}, LaTiO_3 ^{5,6,7,8,9} or YVO_3 ^{10,11,12,13,14,15}. In such systems a large number of states may be nearly degenerate leading to very unusual magnetic properties as for example *colossal magnetoresistance*³ or *magnetization reversals* with temperature^{11,12} but making on the other hand a microscopic description extremely difficult.

From a theoretical point of view most interest has focussed on one-dimensional (1D) versions of the *Kugel-Khomskii Hamiltonian*¹ which allow for a full quantum mechanical treatment. The simplest and most symmetric model describing an $S = 1/2$ spin system with a twofold orbital degeneracy is derived if anisotropies in the orbital sector which are present due to Hund's rule coupling are completely ignored. In this case the Hamiltonian is given by

$$H = \sum_i \left(\mathbf{S}_i \mathbf{S}_{i+1} + \frac{1}{4} \right) \left(\boldsymbol{\tau}_i \boldsymbol{\tau}_{i+1} + \frac{1}{4} \right) \quad (1)$$

where $\tau = 1/2$ is an *orbital pseudospin* describing the occupation of two degenerate orbitals. The model has not only the obvious $SU(2) \times SU(2)$ symmetry, i.e. $SU(2)$ symmetry in both spin and pseudospin space, but also $SU(4)$ symmetry unifying the spin and orbital degrees of freedom.^{16,17} The model is equivalent to the integrable

$q = 4$ Uimin-Sutherland model, which has been solved by Bethe ansatz.¹⁸ The exact ground state and the excitation spectrum consisting of three gapless mixed spin-orbital modes has been obtained. Thermodynamic properties of the $SU(4)$ symmetric model in 1D have been investigated by the quantum Monte Carlo method.¹⁹ In a real compound, however, symmetry will always be reduced due to Hund's rule coupling. A widely studied toy model to investigate the physical consequences of symmetry breaking is given by

$$H = \sum_i (\mathbf{S}_i \mathbf{S}_{i+1} + x) (\boldsymbol{\tau}_i \boldsymbol{\tau}_{i+1} + y) \quad (2)$$

with real constants x, y .^{16,17,19,20,21,22,23} The model is $SU(2) \times SU(2)$ symmetric and exhibits an additional Z_2 symmetry, interchanging spin and orbital degrees of freedom, if $x = y$. The ground-state phase diagram depending on x, y shows 5 phases^{17,21,22,23}: a phase with fully polarized ferromagnetic spins and orbitals (I), phases with antiferromagnetic spin and ferromagnetic orbital states (II) and vice versa (III), a dimerized phase (IV) and a gapless phase (V) which shows $SU(4)$ symmetry at low energies up to a rescaling of the spin and orbital velocities (see Fig. 1).

In this paper we will study thermodynamic properties of the Hamiltonian (2) at the $SU(4)$ -symmetric point, at $x = 0.1, y = 0.25$ and at $x = 0.5, y = 0.5$ which are representative for the gapless phase (V) and for the dimerized phase (IV), respectively. We will focus on two aspects: First we will show that all thermodynamic data at low temperatures (low-T) are consistently described by conformal field theory (CFT) if the system is critical at $T = 0$. Second we will show that the model is highly susceptible for dimerization at *finite temperature* even if the ground state is not dimerized. The outline is as follows: In section II we will briefly introduce the transfer-matrix renormalization group (TMRG) which is the numerical method used to study the model at finite temperatures. We will discuss our results for the $SU(4)$ -symmetric case in section III before we turn to the point $x = 0.1, y = 0.25$ (gapless phase) in IV and to $x = 0.5, y = 0.5$ (dimerized phase) in V. A short summary and

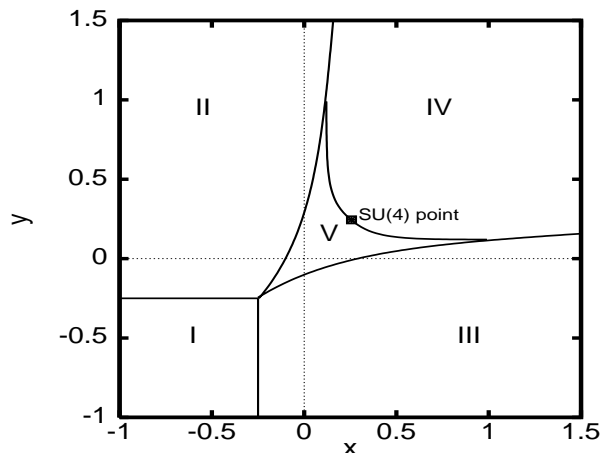


FIG. 1: Phase diagram for the model (2) taken from Ref. 17. Five phases exist as described in the main text.

some conclusions are given in section VI.

II. TRANSFER-MATRIX RENORMALIZATION GROUP

The idea of the TMRG is to express the partition function Z of a one-dimensional quantum model by that of an equivalent two-dimensional classical model which can be derived by the Trotter-Suzuki formula.^{24,25} For the classical model a suitable transfer-matrix can be defined which allows for the calculation of all thermodynamic quantities in the *thermodynamic limit* by considering solely the largest eigenvalue of this transfer matrix. Here we will use the Trotter-Suzuki mapping introduced in Refs. 26,27 which yields

$$Z = \lim_{M \rightarrow \infty} \text{Tr} \left\{ [T_1(\epsilon) T_2(\epsilon)]^{M/2} \right\}$$

with $T_{1,2}(\epsilon) = T_{R,L} \exp[-\epsilon H + \mathcal{O}(\epsilon^2)]$ (3)

where $\epsilon = \beta/M$,³⁸ β being the inverse temperature and M an integer number. $T_{R,L}$ denotes the right- and left-shift operator, respectively. This mapping allows for the definition of a transfer matrix with repeat length 1 and the free energy in the thermodynamic limit is then given by

$$f_M = -T \ln \Lambda_0, \quad (4)$$

where Λ_0 is the largest eigenvalue of the column-to-column transfer matrix T_M . This eigenvalue is non-degenerate and real for any finite temperature. Correlation lengths (CLs) ξ_n are also easy to calculate within this approach. They are given by

$$\xi_n^{-1} = \ln \left| \frac{\Lambda_0}{\Lambda_n} \right|, \quad k_n = \arg \left(\frac{\Lambda_n}{\Lambda_0} \right). \quad (5)$$

where Λ_n are next-leading eigenvalues of T_M and k_n is the corresponding wave vector. The appearance of in principle infinitely many CLs can be understood as follows: Every two-point correlation function can be expanded as

$$\langle O_1 O_r \rangle - \langle O_1 \rangle \langle O_r \rangle = \sum_n M_n e^{-r/\xi_n} e^{ik_n r} \quad (6)$$

with *matrix elements* M_n where O_i denotes some operator at site i . The long distance behavior is dominated by the CL ξ_α belonging to the largest eigenvalue Λ_α ($\alpha \neq 0$) which satisfies the condition $M_\alpha \neq 0$. Note that several CLs ξ with the same wave vector k can appear in this asymptotic expansion. In the structure factor each exponential term yields an (in principle) measurable Lorentz function with center at k_n , height $\sim M_n \xi_n / \pi$ and width $\sim 2/\xi_n$. The sharpest peak corresponds to the leading instability towards the onset of long range order and hence, a crossover in the leading CL indicates a change of the nature of the long range order. The transfer matrix is enlarged in imaginary time direction (being equivalent to a decrease in temperature) by using a density matrix renormalization group (DMRG) algorithm. In all following calculations we have always retained between 350 and 512 states. For details of the algorithm the reader is referred to Refs. 26,28,29,30.

III. THE $SU(4)$ SYMMETRIC POINT

Although thermodynamic properties of the $SU(4)$ symmetric model have already been studied using quantum Monte Carlo algorithms,¹⁹ we will start with this special point for several reasons. First, it provides a good test for the numerics because a comparison with Bethe ansatz and CFT results is directly possible. Second, there are still interesting properties of this model at finite temperature which have not been addressed so far: By comparing the numerically calculated specific heat, spin susceptibility and the correlation length data we will show that even in this highly symmetric case the system is susceptible for dimerization at finite temperature. We will also show that CFT describes consistently all data in the low temperature limit.

In Fig. 2 the free energy f calculated by the TMRG method is shown. The low-energy properties of the model are known to be described by the universality class of the $SU(4)_1$ Wess-Zumino-Witten (WZW) model,^{17,31} equivalent to 3 free boson modes so that we expect from CFT in the low-T limit

$$f = e_0 - \frac{\pi c}{6v} T^2 \quad (7)$$

with *central charge* $c = 3$. The velocity of the elementary excitations $v = \pi/8$ and the ground state energy $e_0 \approx -0.20628$ are known from BA.¹⁸ Eq. (7) is in excellent agreement with the numerics for $T/J < 0.1$. The inset of Fig. 2 displays the entropy $S = -\partial f / \partial T$

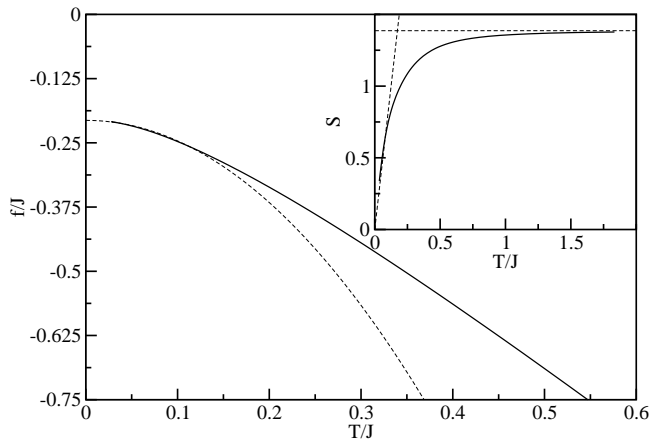


FIG. 2: Free energy (solid line) and low-T asymptotics (dashed line) $f \sim e_0 - 4T^2$ as expected from CFT with e_0 as specified in the text. The inset shows the entropy (solid line) with dashed lines denoting the low ($S \sim 8T$) and high-T asymptotics ($S \sim \ln 4$).

which should be given in the low-T limit by $S \sim 8T$ according to Eq. (7) and by $S \sim \ln 4$ at high temperatures also in good agreement with the numerics. The specific heat calculated by taking the numerical derivative $C = -T\partial^2 f/\partial T^2$ is shown in Fig. 3. Somewhat

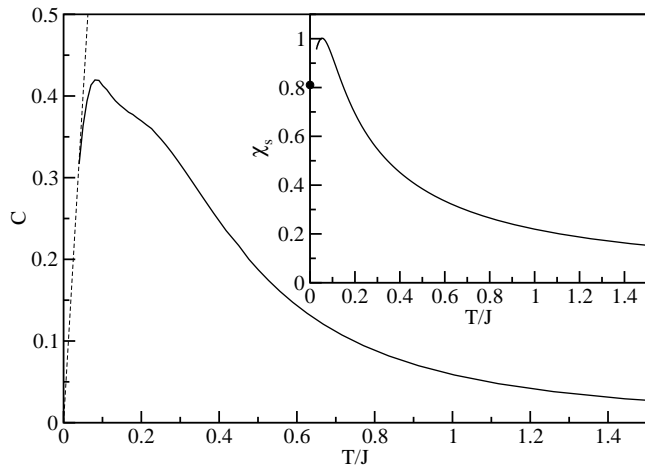


FIG. 3: Specific heat as a function of temperature (solid line) where the dashed line denotes again the low-T asymptotic behavior $C \sim 8T$. In the inset the spin susceptibility is shown and the dot denotes the value expected from CFT.

surprisingly we find apart from a pronounced peak at $T/J \approx 0.08$ an additional shoulder at $T/J \approx 0.22$. We will return to this point soon but first discuss the spin susceptibility χ_s ³⁹ at magnetic field $h = 0$ which is shown in the inset of Fig. 3. This quantity is calculated numerically by $\chi_s|_{h=0} = m/h$ where h is a small applied magnetic field of the order $J/100$ and m is the corresponding magnetization which can be calculated directly

within TMRG.²⁸ To calculate $\chi_s(T = 0)$ within CFT one has to remind that the $SU(4)_1$ WZW model is equivalent to a sum of 2 decoupled $SU(2)_2$ WZW models.^{17,31} This model is therefore a rare example of a critical spin model with Kac-Moody central charge $k > 1$. It has been conjectured³² that the susceptibility of an isotropic spins antiferromagnet will be given by $\chi_s = k/2\pi v_s$ so that we expect $\chi_s = 1/\pi v_s = 8/\pi^2$ which is in good agreement with a linear extrapolation of the numerical result to $T = 0$.

By comparing C and χ_s which show both a peak in the same temperature region $T/J \approx 0.08$ we could identify this peak as due to the elementary excitations of the $SU(4)_1$ WZW model. Note also that this peak marks the point in temperature where the asymptotic expressions from CFT shown in Figs. 2 and 3 become invalid. To understand the appearance of the shoulder we note that the energy for a single bond is given by $-J/4$ if the spins form a singlet (triplet) and the orbitals a triplet (singlet) and by $+J/4$ if both are in singlet or triplet configuration. Therefore the excitation energy δ for a single bond is $\delta = J/2$. In thermodynamic data, however, it makes no difference for unbound excitations if they appear in pairs or not so that the energy scale is set by $\delta/2 = J/4$. This approximately coincides with the shoulder in Fig. 3. So we may attribute this structure to the excitations of a chain with short range dimer order in both spin and orbital sector which seems to form at finite temperature although the ground state is not dimerized. This picture is further supported by an investigation of the leading CLs which are plotted as $T\xi/J$ in Fig. 4 because a $1/T$ divergence at low-T of those CLs belonging to the critical modes is expected (see below). Here a CL ξ_D is present (dot-dashed line) which appears

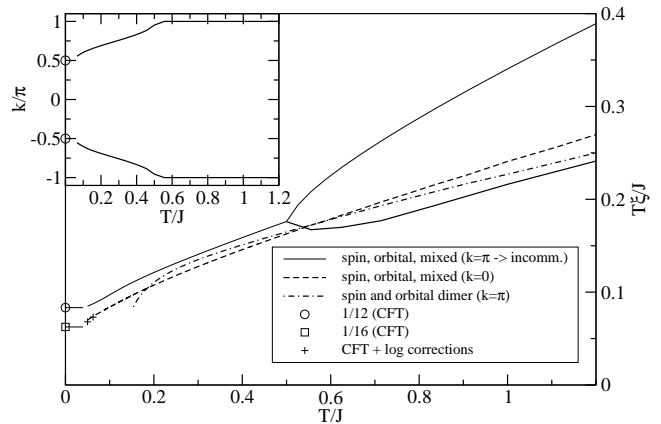


FIG. 4: Leading correlation lengths at the $SU(4)$ -point. The symbols at $T = 0$ are CFT results where the short lines should indicate that these results are expected to be valid (up to log. corrections) also at small but finite temperatures. The inset shows the temperature dependence of the wave vector k in the case of incommensurate oscillations.

in the asymptotic expansion (Eq. (6)) of the dimer correlation functions $\langle S_0^z S_1^z S_r^z S_{r+1}^z \rangle$ and $\langle \tau_0^z \tau_1^z \tau_r^z \tau_{r+1}^z \rangle$. ξ_D is

in $T/J \in [0.2 : 0.5]$ only slightly smaller than the largest CL supporting the picture of a short range dimer order in this temperature regime. For lower temperatures $T\xi_D$ starts to decrease as is expected because the ground state is not dimerized and ξ_D should therefore remain finite. Note that due to the $SU(4)$ symmetry the relation

$$\langle S_i^\alpha S_j^\alpha \rangle = \langle \tau_i^\alpha \tau_j^\alpha \rangle = 4 \langle S_i^\alpha \tau_i^\beta S_j^\alpha \tau_j^\beta \rangle \quad (8)$$

is valid for the thermodynamic correlation functions with arbitrary components $\alpha, \beta = x, y, z$.¹⁶ Therefore the CLs depicted in Fig. 4 as straight and dashed lines have connected non-zero matrix elements for the spin-spin, orbital-orbital and mixed spin-orbital correlator. At high temperatures these CLs show commensurate oscillations, i.e., the wave vector k is equal 0 or π . The 2 CLs which show π -oscillations at high temperatures (straight lines in Fig. 4) merge at a temperature $T/J \sim 0.5$ with a square root singularity (note that the number of data points is relatively small in this region) and the oscillations become incommensurate and temperature dependent at lower temperatures as shown in the inset of Fig. 4. A similar behavior has been observed for the longitudinal spin CL in the XXZ -model for finite magnetic field.³³ Note that incommensurate oscillations are associated with a pair of complex conjugate eigenvalues of the transfer matrix (see Eq. (5)) which can occur because the transfer matrix is real but non-symmetric. Additionally a CL (dashed line) is present which is non-oscillating for all temperatures.

It is known that the energy levels E_i of a finite chain of length L show a finite-size scaling behavior

$$E_i - E_0 = \frac{2\pi v x_i}{L} \quad (9)$$

where E_0 is the ground state energy and x_i is the scaling dimension of the operator leading to the excited state with energy E_i .³⁴ We can get the corresponding result for an infinite chain at *finite* temperature by the substitution $L \rightarrow v/T$. This leads to

$$\xi_i^{-1} = \ln \Lambda_0 - \ln |\Lambda_i| = \frac{2\pi x_i T}{v} \quad (10)$$

where Λ_i, Λ_0 are eigenvalues of the transfer matrix. The possible scaling dimensions for an $SU(N)$ symmetric model are given by $x_p = p(N-p)/N$ with $p = 1, 2, \dots, N-1$. The dominant mode belongs to $p = 1$ and oscillates at zero temperature with $k = 2\pi/N$.^{31,35} In the case of $SU(4)$, scaling dimensions $3/4, 1, 3/4$ are therefore possible and the dominant mode has $x = 3/4$ and oscillates with $k = \pi/2$. Using Eq. (10) we obtain $\xi_{\pi/2} = 1/12T$. The non-oscillating CL must belong to the second possible scaling dimension $x = 1$ leading to $\xi_0 = 1/16T$ in the low-T regime. However, this $1/T$ behavior will be directly observable only at very low temperatures (see Ref. 19). At the lowest temperatures we are able to access in this study it is covered by logarithmic corrections which are present here due to marginally irrelevant operators in the low-energy effective theory.^{17,35}

Cardy has shown that such logarithmic corrections have universal character and can be displayed in leading order as

$$E_i - E_0 = \frac{2\pi v}{L} \left(x_i + \frac{2b_n}{b} \frac{1}{\ln L} \right) \quad (11)$$

where b_n, b are universal numbers.³⁶ However, it should be stressed that this asymptotic form is only observable for very large chain lengths L when the logarithmic correction becomes independent of the coupling constant g of the considered marginal operator. Otherwise we can only replace g by its renormalization group improved value $g(\ln L)$ so that we must substitute $\ln L \rightarrow \ln(L/L_0)$ in Eq. (11) with a non-universal L_0 . But even in this case Eq. (11) remains useful because it describes the scaling behavior of *different* excited states by a single parameter. By $L \rightarrow v/T$ we find for the CLs

$$\xi_i^{-1} = \frac{2\pi T}{v} \left(x_i + \frac{2b_n}{b} \frac{1}{\ln T_0/T} \right) \quad (12)$$

where T_0 is non-universal. This means that logarithmic corrections lead to an effective temperature dependent correction of the scaling dimension x_i . The universal factor $2b_n/b$ for the $SU(4)$ model has been derived in Ref. 35 and is given by $2b_n/b = -1/16$ for scaling dimension $x = 3/4$ and by $2b_n/b = -1/4$ for $x = 1$. Therefore the logarithmic correction for ξ_0 is more important than that for $\xi_{\pi/2}$ in qualitative agreement with the data. To illustrate more quantitatively that the logarithmic corrections can explain the deviations from the expected CFT values, we have estimated T_0 at $T = 0.05J$ and $T = 0.0625J$ for $\xi_{\pi/2}$ by applying Eq. (12) and used this value to calculate ξ_0 at the same temperature. The results are depicted as plus-symbols in Fig. 4 and are in good agreement with the numerically calculated ξ_0 . We like to remark that this is a very sensitive test because T_0 depends exponentially on ξ . Note also that we cannot extend this comparison between field theory and numerics to larger temperatures because we already know that the low energy effective theory breaks down at least at $T/J \approx 0.08$.

IV. GAPLESS PHASE ($SU(4)$ WITH RESCALED VELOCITIES)

By an RG analysis it has been shown that the Hamiltonian (2) is not only critical at the $SU(4)$ -symmetric point but rather exhibits an extended region in phase space around this point which is gapless (phase V in Fig.1).^{17,22} Considering the parameters $x = 1/4 + \delta x$, $y = 1/4 + \delta y$ in Eq. (2), where $\delta x, \delta y$ are small perturbations, the findings can be summarized as follows: (1) For $\delta x = \delta y < 0$ the breaking of the $SU(4)$ symmetry down to $SU(2) \times SU(2)$ is irrelevant and the low-energy behavior is still described by the $SU(4)_1$ WZW model. (2) $\delta x + \delta y < 0$ with $\delta x \neq \delta y$ is marginally irrelevant and the

critical theory is the $SU(2)_2 \times SU(2)_2$ WZW model with *unequal* velocities v_s, v_o , but with unchanged scaling dimensions. (3) $\delta x + \delta y > 0$ is marginally relevant leading to a Kosterlitz-Thouless type transition into a dimerized phase (phase IV in Fig.1).

Representatively for the gapless phase with unequal velocities of the elementary excitations we will study the point $x = 0.1, y = 0.25$. Due to the different velocities $v_s \neq v_o$ relation (8) is no longer valid and the degeneracy between spin-spin, orbital-orbital and mixed spin-orbital CLs is lifted. This makes the situation far more complex than in the $SU(4)$ case with numerous crossovers between different CLs occurring in the non-universal regime at elevated temperatures. To keep it concise we show only a selection of CLs at high temperatures in Fig. 5 and show the 6 largest CLs at the lowest numerically accessible temperatures separately in Fig. 6. Over a wide temper-

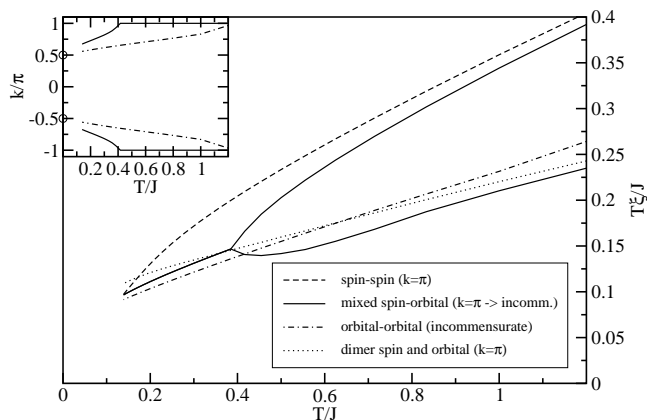


FIG. 5: Some of the leading spin and orbital correlation lengths for $(x, y) = (0.1, 0.25)$. The wave vectors are shown in the inset if incommensurate oscillations occur. The circles in the inset denote $\pm\pi/2$.

ature range a π -oscillating spin CL is leading. This is expected because antiferromagnetic spin correlations are stabilized with decreasing x . As in the $SU(4)$ -symmetric case two CLs with π -oscillations merge at a temperature $T/J \sim 0.4$ and show incommensurate oscillations below which approach $\pi/2$ at $T = 0$. However, in the $SU(4)$ case these CLs are threefold degenerate belonging to spin, orbital and mixed spin-orbital correlation functions. Here no degeneracy is present and the CLs only belong to the mixed spin-orbital correlator. The orbital CL which shows $\pi/2$ oscillations at $T = 0$ develops incommensurability already at higher temperatures as shown in the inset of Fig. 5. Hitherto we have ignored the dimer CL ξ_D which is not only one of the largest CL as in the $SU(4)$ case but is indeed leading in a certain temperature range. This is a little bit astonishing because we have moved away from the dimer phase by $\delta x < 0$. It shows that the spin-orbital model has an intrinsic tendency towards dimerization at finite temperature even in regions of phase space where the ground state is not dimerized.

For a system consisting of weakly coupled spin-orbital chains this suggests that long range dimer order can be stabilized at finite temperature and that such a system may show a phase transition from a dimer phase in this temperature regime to a non-dimerized phase at lower temperatures. In the limit $T \rightarrow 0$ we expect that ξ_D remains finite and Fig. 6 shows indeed a decreasing $T\xi_D$. However, even at the lowest numerically accessible temperature ξ_D is still the second largest CL. Dominating at

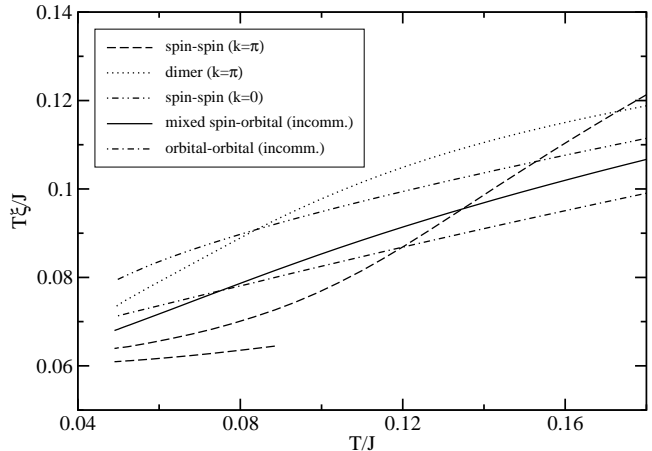


FIG. 6: Leading spin and orbital correlation lengths for $(x, y) = (0.1, 0.25)$ at low temperatures.

low temperatures is a non-oscillating spin CL. Furthermore we see a crossover between the mixed spin-orbital and the orbital-orbital CL with incommensurate oscillations with the orbital-orbital CL becoming the larger one at low- T . From CFT we also expect a spin-spin CL with incommensurate oscillations which seems to be missing in our data. We expect that the 2 spin-spin CLs with $k = \pi$ depicted as dashed lines in Fig. 6 will merge at lower temperature yielding this missing CL. This implies that we still have not reached the temperature regime where the behavior of the CLs becomes universal and can be described by CFT. Therefore we cannot compare the numerics with CFT in detail. However, assuming that we are close to the conformal regime and ignoring logarithmic corrections completely we can extrapolate all CLs (except of the dimer CL) shown in Fig. 6 starting from the numerical data at the lowest accessible temperature according to their expected $1/T$ behavior. This allows us to show that the data are in rough agreement with CFT.

The non-oscillating spin-spin CL must belong to an excitation with $x_s = 1$ so that $\xi = v_s/2\pi T$ leading to $v_s \approx 0.5$. For the corresponding non-oscillating orbital-orbital CL we find numerically (data not shown) $\xi(T = 0.047) \approx 0.86$ leading to $v_o \approx 0.25$. We expect that the $SU(4)$ representation is decomposed symmetrically into a spin and orbital sector both with central charge $c = 3/2$ and fundamental fields with scaling dimensions $x = 3/8$. The only difference between the two sectors

are the velocities. All CLs with $k = \pi/2$ at $T = 0$ are therefore given by an excitation with $x_s = x_o = 3/8$ so that we expect from CFT

$$\xi_{\pi/2} = \frac{1}{2\pi\frac{3}{8}(\frac{1}{v_s} + \frac{1}{v_o})T} \sim \frac{0.071}{T} \quad (13)$$

where we have substituted the velocities v_s , v_o which we have determined from the non-oscillating spin and orbital CL. At finite temperatures the mixed, spin and orbital CL with incommensurate oscillations differ from each other because each has different logarithmic corrections.¹⁷ We notice that the value estimated in Eq. (13) is indeed in rough agreement with the numerical data at the lowest accessible temperature (see Fig. 6). The mixed spin-orbital CL with $k = 0$ is given by an excitation with $x_s = x_o = 1/2$ leading to

$$\xi_0^{s-o} = \frac{1}{2\pi\frac{1}{2}(\frac{1}{v_s} + \frac{1}{v_o})T} \sim \frac{0.053}{T} \quad (14)$$

predicting $\xi_0^{s-o}(T = 0.047) \approx 1.12$ which is in good agreement with the numerically calculated value $\xi_0^{s-o}(T = 0.047) \approx 1.09$ (data not shown).

The CFT result for the free energy of the $SU(4)$ -symmetric model (Eq. (7)) can be easily generalized to the case of $SU(2) \times SU(2)$ -symmetry with different velocities

$$f = e_0 - \frac{\pi c}{6} \left(\frac{1}{v_s} + \frac{1}{v_o} \right) T^2 \quad (15)$$

where now $c = 3/2$. In Fig. 7 the numerically calculated free energy and the low-T asymptotics according to this formula are shown. Here we have used the spin and orbital velocities which we have evaluated from the CLs and e_0 as a fitting parameter. We find $e_0 \approx -0.2197J$ and a

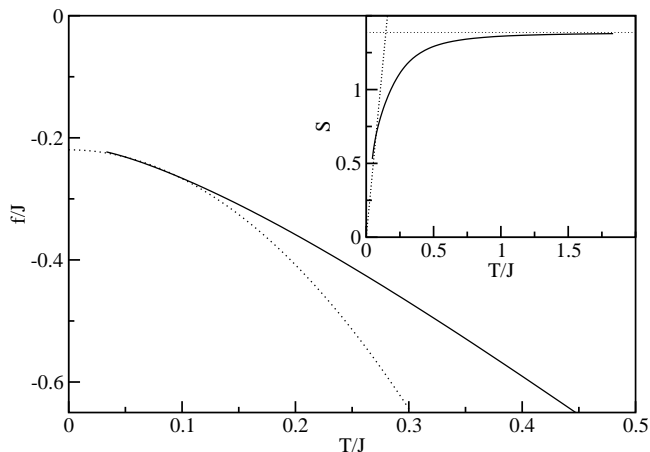


FIG. 7: Free energy and entropy (inset) at $(x, y) = (0.1, 0.25)$ with low and high-T asymptotics (dotted lines) as described in the text.

good agreement with the numerical data for $T/J < 0.1$.

In the inset of Fig. 7 the entropy and the low-T ($S \sim 3\pi T$) and high-T asymptotics ($S \sim \ln 4$) are shown. Here the low-T asymptotics is determined solely by the spin and orbital velocities without any additional fitting parameter showing that CFT for the $SU(2) \times SU(2)$ model with our velocity estimates gives a consistent description of all thermodynamic quantities at low energies. Next we want to consider the specific heat C shown in Fig. 8. Contrary to the $SU(4)$ -symmetric case not only a peak

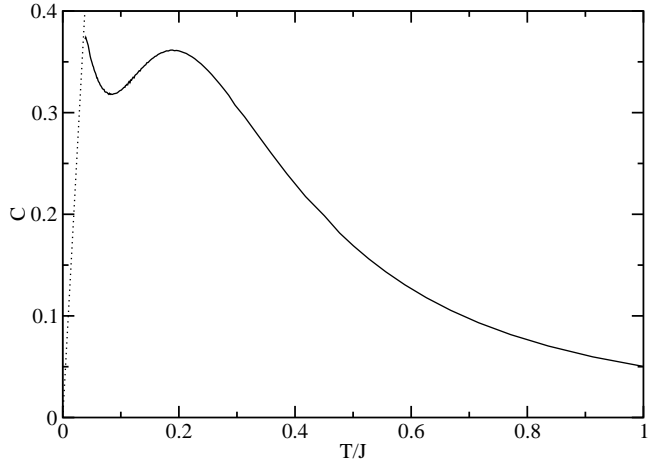


FIG. 8: Specific heat (solid line) and low-T asymptotics (dashed line) $C \sim 3\pi T$ at $(x, y) = (0.1, 0.25)$.

and a shoulder but instead two clearly distinguishable peaks are visible. Note that due to the different velocities, orbital and spin excitations have now different energy scales. However, any saturation of one type of elementary excitations (spinons or orbitons) will inevitably destroy also a description in terms of these elementary excitations for the other sector due to the strong coupling between both. That this is indeed the case is obvious from the susceptibility data shown in Fig. 9 which show that spin and orbital susceptibility are peaked approximately at the same temperature.⁴⁰ The second peak of C is in a temperature range where short range dimer order exists and may be attributed to excitations connected to this. Finally we want to compare the susceptibility data with CFT. As in the $SU(4)$ case we expect $\chi_{s,o} = k/2\pi v_{s,o}$ with topological coupling constant $k = 2$, however, now $v_s \neq v_o$. Using the velocity estimates from the fit of the CLs we find $\chi_s \approx 2/\pi$ and $\chi_o \approx 4/\pi$ predicting χ_o at $T = 0$ being twice as large as χ_s . Although we cannot access numerically temperatures low enough to show that the susceptibilities converge to these values as $T \rightarrow 0$ we note that χ_o is indeed more than twice as large as χ_s at low temperatures.

V. DIMERIZED PHASE

As described in the previous section perturbing the $SU(4)$ -symmetric Hamiltonian by $\delta x + \delta y > 0$ is

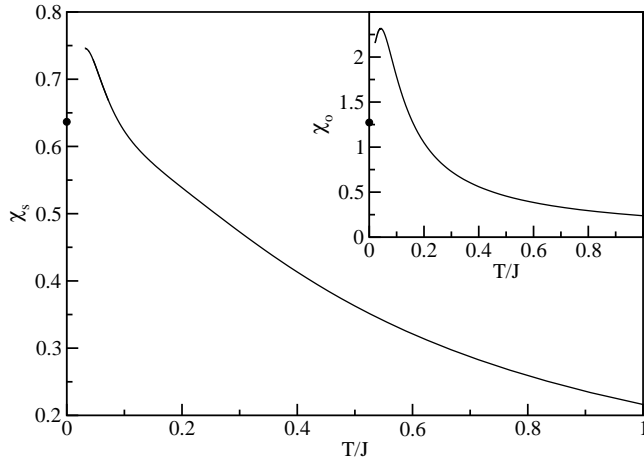


FIG. 9: Spin (main figure) and orbital (inset) susceptibilities at $(x, y) = (0.1, 0.25)$. The dots denote CFT results as described in the text.

marginally relevant. As a result a gap Δ in the excitation spectrum is expected. Here we do not want to investigate this phase transition in detail but rather restrict ourselves to study the point $x = 0.5, y = 0.5$ as a representative for the dimerized phase. First, consider the spin susceptibility χ_s shown in Fig. 10. A

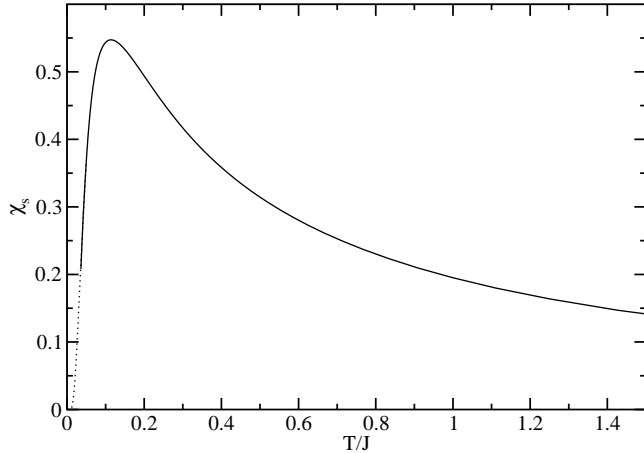


FIG. 10: Susceptibility (solid line) for $(x, y) = (0.5, 0.5)$ where the dotted line denotes the best low-T fit with $S = 0.491 \exp(-0.09/T)/\sqrt{T}$.

sharp peak at $T = 0.12J$ is visible. At lower temperatures χ_s goes to zero as expected for a gapped system. The usual quadratic dispersion of elementary excitations above the gap yields in 1D an expected low-T asymptotic behavior $\chi_s \sim \exp(-\Delta/T)/\sqrt{T}$. Using this formula for a fit of the data in the low-T regime we find $\Delta = 0.090 \pm 0.005$ where we get a certain error estimate by varying the fit interval.⁴¹ This value is in agreement with a recent series expansion study.³⁷ In Fig. 11 the corresponding entropy S is shown. For the free energy we

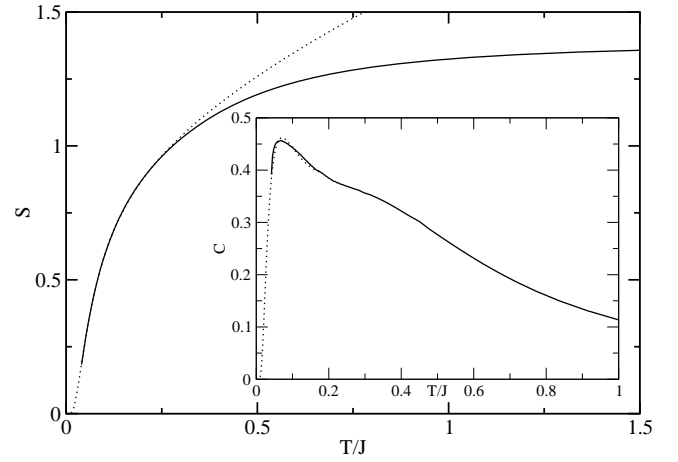


FIG. 11: Entropy and specific heat (inset) at $(x, y) = (0.5, 0.5)$. The dashed lines denote low-T fits as described in the text.

expect at low temperatures $f \sim -T^{3/2} \exp(-\Delta/T)$ leading to $S \sim (A\sqrt{T} + B/\sqrt{T}) \exp(-\Delta/T)$. Using A, B, Δ as parameter in a fit of the numerical data for $T < 0.1J$ we get the result shown as dotted line in Fig. 11 which is an excellent fit even up to $T \sim 0.25J$. From this fit we find $\Delta = 0.094 \pm 0.004$ where the error stems again from a variation of the interval used in the fit. We note that this value is in perfect agreement with the estimate from the susceptibility fit. In the inset of Fig. 11 the specific heat (solid line) is shown. The dotted line denotes the low temperature specific heat calculated from the entropy fit and shows good agreement with the numerical data. Note that the excitation energy δ for a single bond is now $J/4$ so that the peak in the specific heat at approximately $\delta/2$ can be attributed again to excitations of the chain with dimer order which will now become a true long range order at $T = 0$. Surprisingly we still find a shoulder in C at higher temperatures as in the $SU(4)$ case. Comparing with the CLs plotted in Fig. 12 we find indeed that the eigenspectrum of the transfer matrix at elevated temperatures has not changed drastically compared to Fig. 4. Especially, we find again a dimer CL (dot-double dashed line) which becomes the second largest CL in $T/J \in [0.3 : 0.55]$ which coincides with the shoulder in C . Whereas this dimer CL stays finite as $T \rightarrow 0$ another dimer CL (also depicted as dot-dashed line)⁴² is diverging more strongly than $1/T$ indicating long range dimer order at $T = 0$. Because $x = y$ the CLs belonging to the spin and orbital correlation function are equal, however, CLs belonging to the mixed correlator are different in general.⁴³ The two CLs (solid lines) which merge at $T/J \sim 0.5$ yielding a CL with corresponding incommensurate oscillations below that temperature have indeed only non-zero matrix elements for $\langle S_0^z S_r^z \rangle$ and $\langle \tau_0^z \tau_r^z \rangle$. The π -oscillating CLs with non-zero matrix element for $\langle S_0^z \tau_0^z S_r^z \tau_r^z \rangle$ merge already at a higher temperature and the oscillations become incommensurate be-

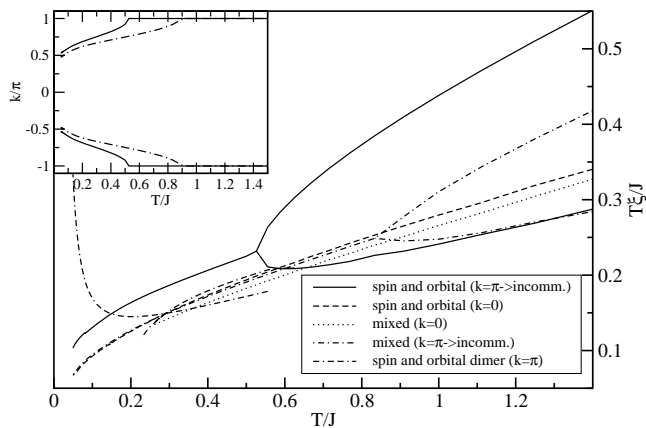


FIG. 12: Leading CLs at $(x, y) = (0.5, 0.5)$. The inset shows the dependence of the wave vector on temperature in the case of incommensurate oscillations.

low as shown in the inset of Fig. 4. Similarly, the largest non-oscillating CL belongs only to the spin and orbital correlator whereas the second largest appears only in the asymptotic expansion of the mixed correlator. The numerical data indicate that all CLs apart from the dimer CL stay finite as $T \rightarrow 0$ which is expected for a system with a gap.

VI. CONCLUSIONS

In summary, we have used the TMRG method to study thermodynamic properties of a spin-1/2 $SU(2) \times SU(2)$ spin-orbital model. We have concentrated on three representative points in the phase diagram: (1) The $SU(4)$ symmetric point where the model is Bethe-ansatz integrable and shows critical properties at $T = 0$, (2) a point where the model still exhibits critical behavior at zero temperature, however, the symmetry is reduced to $SU(2) \times SU(2)$, and (3) a point where the ground state has long range dimer order.

In the first two cases we have compared our numerical results in detail with CFT in the low temperature regime and with special attention to the evolution of various CLs with temperature. In both cases three different regimes could be identified: At elevated temperatures crossovers between different CLs are frequent and the corresponding wave vectors are commensurate. The π -oscillating CLs belonging to the spin, orbital or mixed spin-orbital correlator merge at a certain temperature with a square root singularity and the oscillations become incommensurate and temperature dependent below which characterizes the intermediate temperature regime. Finally, at low

temperatures the conformal invariant regime is reached where the CLs belonging to critical excitations diverge as $1/T$ up to logarithmic corrections and no crossover occur. The comparison of the numerics with CFT was especially simple at the $SU(4)$ point because the velocities of the elementary excitations are known exactly from Bethe ansatz.¹⁸ In this case we have also been able to show that the predicted logarithmic corrections^{17,35} account quantitatively for the observed deviations from a pure $\xi \sim 1/T$ behavior at low temperatures. In the second case a comparison with CFT was far more complicated as the velocities v_s, v_o are a priori unknown and several crossovers in the lowest numerically accessible temperature region show that the conformal invariant regime was not reached. However, we have been able to get rough estimates for the spin and orbital velocities from the CLs and have shown that these estimates give a consistent description of other thermodynamic quantities within CFT.

For the point in the dimerized phase we have calculated the gap from the susceptibility and entropy data and have found good agreement with a recent series expansion study.³⁷ More important, we have found that the behavior of CLs in the high and intermediate temperature regime here is quite similar to the gapless phase. At low temperatures a dimer CL diverges more strongly than $1/T$ whereas all other CLs stay finite as is expected for a system with long range dimer order at $T = 0$.

Most surprisingly we find in all 3 cases a strong tendency towards dimerization in a certain finite temperature interval and dimerization could be the leading instability in this region even if the ground state is not dimerized. This behavior is very similar to what was observed recently in another spin-orbital model with spin $S = 1$ ¹⁴ indicating that such instability may be an intrinsic property of these kind of Kugel-Khomskii Hamiltonians. In a system of weakly coupled spin-orbital chains this instability may turn into true long range dimer order at finite temperature. More generally speaking, it indicates that even a pure electronic model may show various temperature driven phase transitions between different spin and orbital orderings due to the large number of nearly degenerated states accessible to systems with unquenched orbital degrees of freedom.

Acknowledgments

I thank A. Klümper and J. Oitmaa for useful discussions. This work has been partially supported by the DFG in SP1073 and by the Australian Research Council. The numerical calculations were partially performed using the APAC computing facilities.

* sirker@phys.unsw.edu.au

¹ K. I. Kugel and D. I. Khomskii, Sov. Phys. Usp. **25**, 231

- (1982).
- ² Y. Tokura and N. Nagaosa, *Science* **288**, 462 (2000).
 - ³ Y. Tokura, ed., *Colossal Magnetoresistive Oxides* (Gordon and Breach Science, New York 2000), and references therein.
 - ⁴ J. M. D. Coey, M. Viret, and S. von Molnár, *Adv. Phys.* **48**, 167 (1999).
 - ⁵ G. Khaliullin and S. Maekawa, *Phys. Rev. Lett.* **85**, 3950 (2000).
 - ⁶ B. Keimer, D. Casa, A. Ivanov, J. W. Lynn, M. v. Zimmermann, J. P. Hill, D. Gibbs, Y. Taguchi, and Y. Tokura, *Phys. Rev. Lett.* **85**, 3946 (2000).
 - ⁷ J. Hemberger, H.-A. K. von Nidda, V. Fritsch, J. Deisenhofer, S. Lobina, T. Rudolf, P. Lunkenheimer, F. Lichtenberg, A. Loidl, D. Bruns, et al., *Phys. Rev. Lett.* **91**, 066403 (2003).
 - ⁸ M. Cwik, T. Lorenz, J. Baier, R. Müller, G. André, F. Bourée, F. Lichtenberg, A. Freimuth, R. Schmitz, E. Müller-Hartmann, et al., *Phys. Rev. B* **68**, 060401 (2003).
 - ⁹ M. Mochizuki and M. Imada, *Phys. Rev. Lett.* **91**, 167203 (2003).
 - ¹⁰ G. Khaliullin, P. Horsch, and A. M. Oleś, *Phys. Rev. Lett.* **86**, 3879 (2001).
 - ¹¹ Y. Ren, T. T. M. Palstra, D. I. Khomskii, A. A. Nugroho, A. A. Menovsky, and G. A. Sawatzky, *Phys. Rev. B* **62**, 6577 (2000).
 - ¹² Y. Ren, T. T. M. Palstra, D. I. Khomskii, E. Pellegrin, A. A. Nugroho, A. A. Menovsky, and G. A. Sawatzky, *Nature* **396**, 441 (1998).
 - ¹³ M. Noguchi, A. Nakazawa, S. Oka, T. Arima, Y. Wakabayashi, H. Nakao, and Y. Murakami, *Phys. Rev. B* **62**, R9271 (2000).
 - ¹⁴ J. Sirker and G. Khaliullin, *Phys. Rev. B* **67**, 100408(R) (2003).
 - ¹⁵ C. Ulrich, G. Khaliullin, J. Sirker, M. Reehuis, M. Ohl, S. Miyasaka, Y. Tokura, and B. Keimer, *Phys. Rev. Lett.* (2003), in print.
 - ¹⁶ Y. Q. Li, M. Ma, D. N. Shi, and F. C. Zhang, *Phys. Rev. Lett.* **81**, 3527 (1998).
 - ¹⁷ C. Itoi, S. Qin, and I. Affleck, *Phys. Rev. B* **61**, 6747 (2000).
 - ¹⁸ B. Sutherland, *Phys. Rev. B* **12**, 3795 (1975).
 - ¹⁹ B. Frischmuth, F. Mila, and M. Troyer, *Phys. Rev. Lett.* **82**, 835 (1999).
 - ²⁰ Y. Yamashita, N. Shibata, and K. Ueda, *Phys. Rev. B* **58**, 9114 (1998).
 - ²¹ S. K. Pati and R. R. P. Singh, *Phys. Rev. B* **61**, 5868 (2000).
 - ²² P. Azaria, E. Boulat, and P. Lecheminant, *Phys. Rev. B* **61**, 12112 (2000).
 - ²³ S. K. Pati, R. R. P. Singh, and D. I. Khomskii, *Phys. Rev. Lett.* **81**, 5406 (1998).
 - ²⁴ H. F. Trotter, *Proc. Amer. Math. Soc.* **10**, 545 (1959).
 - ²⁵ M. Suzuki, *Phys. Rev. B* **31**, 2957 (1985).
 - ²⁶ J. Sirker and A. Klümper, *Europhys. Lett.* **60**, 262 (2002).
 - ²⁷ J. Sirker and A. Klümper, *Phys. Rev. B* **66**, 245102 (2002).
 - ²⁸ I. Peschel, X. Wang, M. Kaulke, and K. Hallberg, eds., *Density-Matrix Renormalization, Lecture Notes in Physics*, vol. 528 (Springer, Berlin, 1999), and references therein.
 - ²⁹ X. Wang and T. Xiang, *Phys. Rev. B* **56**, 5061 (1997).
 - ³⁰ N. Shibata, *J. Phys. Soc. Jpn.* **66**, 2221 (1997).
 - ³¹ I. Affleck, *Nucl. Phys. B* **265**, 409 (1986).
 - ³² I. Affleck, *Phys. Rev. Lett.* **56**, 2763 (1986).
 - ³³ A. Klümper, J. R. R. Martinez, C. Scheeren, and M. Shi-roishi, *J. Stat. Phys.* **102**, 937 (2001).
 - ³⁴ J. L. Cardy, *J. Phys. A* **17**, L385 (1984).
 - ³⁵ K. Majumdar and M. Mukherjee, *J. Phys. A* **35**, L543 (2002).
 - ³⁶ J. L. Cardy, *J. Phys. A* **19**, L1093 (1986).
 - ³⁷ W. Zheng and J. Oitmaa, *Phys. Rev. B* **64**, 014410 (2001).
 - ³⁸ Within this paper we will use $\epsilon = 0.05$ in all calculations.
 - ³⁹ Note that spin and orbital susceptibility are equal along the line $x = y$.
 - ⁴⁰ More precisely, χ_o is peaked at $T \approx 0.043J$ and χ_s at $T \approx 0.033J$.
 - ⁴¹ This error does not include systematic errors due to the truncation of the Hilbert space which are difficult to estimate.
 - ⁴² We use the same symbol for both CLs because they are of the same type. However, they are connected to different eigenvalues which are crossing at a certain temperature.
 - ⁴³ Eq. (8) is not valid here.